Self-Doped Conducting Polymer as a Hole-Extraction Layer in Organic–Inorganic Hybrid Perovskite Solar Cells

*Kyung-Geun Lim, Soyeong Ahn, Hobeom Kim, Mi-Ri Choi, Dal Ho Huh, and Tae-Woo Lee**

Organic–inorganic hybrid perovskite solar cells are fabricated using a water-soluble, self-doped conducting polyaniline graft copolymer based on poly(4-styrenesulfonate)-*g*-polyaniline (PSS-*g*-PANI) as an efficient hole-extraction layer (HEL) because of its advantages, including low-temperature solution processability, high transmittance, and a low energy barrier with perovskite photoactive layers. Compared with conventional poly(3,4-ethylenedioxythiophene):poly(styrene sulfonate) (PEDOT:PSS) dispersed in water solution, PSS-*g*-PANI molecules are dissolved in water because of the polymeric dopant covalently bonded with PANI, and can steadily remain as an initial solution during long-term storage and over a wide pH range to fabricate a HEL with fewer surface defects. The built-in potential and device characteristics are substantially improved because of the surface energy state of PSS-*g*-PANI below Fermi-energy level. Moreover, the PSS-*g*-PANI mixed with electron-withdrawing perfluorinated ionomer (PFI) exhibits a higher work function (5.49 eV) and deeper surface energy state below the Fermi level; thus, an ohmic contact at the HEL/methylammonium lead iodide perovskite interface is obtained. Finally, the power conversion efficiency was increased from 7.8% in the perovskite solar cells with PEDOT:PSS to 12.4% in those with the PSS-*g*-PANI:PFI.

1. Introduction

Power conversion efficiency (PCE) of organic–inorganic hybrid perovskite solar cells (PrSCs) have rapidly increased for a short time[1–10] because the perovskite photoactive layer exhibits outstanding electronic properties,[11,12] controllable band gap and absorption spectra,[13] and high extinction coefficient.[5,14] In early reports, PrSCs included mesoporous TiO_2[1–4,6] as a charge transfer layer or mesoporous Al_2O_3[5] as the insulating scaffold because these PrSCs were based on the structure of dye-sensitized solar cells. Despite the high efficiency of PrSCs with mesoporous charge transfer layer, their application into the flexible electronics would be limited due to their brittleness and the high-temperature (i.e., $T >$ 450 °C) sintering process which damages plastic substrates. Otherwise, solution-processed planar heterojunction (SP-PHJ) PrSCs can be fabricated using low-temperature processable interlayers without mesoporous metal oxides; this approach enables the fabrication of flexible PrSCs on plastic substrates.[7–9] Therefore, the development of a solution-processed and efficiently charge-transporting interlayer material has been required recently to increase PCE of SP-PHJ PrSCs for the practical application of highly efficient and flexible PrSCs. In addition to conducting polymers (e.g., poly(3,4-ethylenedioxythiophene):poly(styrene sulfonate) (PEDOT:PSS),[7,9,15,16] self-organized hole extraction layer (SOHEL)[9]), several different hole transport materials (HTMs), including inorganic materials (graphene oxide,[17] reduced graphene oxide,[18] NiO*x*[15]) and conjugated polymers (e.g., PolyTPD,[19] P3HT,[20] poly(2,5-(2-octyldodecyl)-3,6-diketopyrrolopyrrole-alt-5,5-(2′,5′-di(thien-2-yl)thieno[3,2-b]thiophene) (DPP-DTT),[21] PCP-DTBT,[21] and PCDTBT[21]) have been used to increase the PCE in SP-PHJ PrSCs.

Among these materials, polymeric HTMs have been intensively developed for highly efficient SP-PHJ PrSCs because they can be fabricated by solution processing and exhibit better hole mobility compared to vacuum-processed small-molecule HTMs.[3]

In the first few papers reporting SP-PHJ PrSCs, they were based on the PEDOT:PSS HTM[16] because PEDOT:PSS is one of the most commonly used HTMs for organic photovoltaics[22–27] and organic light-emitting diodes (OLEDs).[28,29] However, work function (WF) of PEDOT:PSS (≈4.9–5.2 eV) is highly dependent on the ratio of the polymeric acid, PSS relative to PEDOT[25,28] and therefore may not be sufficiently high to perfectly match the valence band maxima (VBM) of perovskite materials (e.g., –5.43 eV for methylammonium lead iodide ($MAPbI_3$)) for ohmic contact and consequential efficient charge extraction.[9,15,19–29] Moreover, PEDOT:PSS is dispersed with a large particle size (≈60 nm) in solution;[30] it precipitates slowly from the solution during storage and is difficult to redisperse from the aggregated

Dr. K.-G. Lim, S. Ahn, H. Kim, M.-R. Choi, Prof. T.-W. Lee
Department of Materials Science and Engineering
Pohang University of Science and Technology (POSTECH)
77 Cheongam-Ro, Nam-gu, Pohang
Gyungbuk 790-784, Republic of Korea
E-mail: twlee@postech.ac.kr; taewlees@gmail.com
Dr. D. H. Huh
Samsung SDI Co., Ltd
130, Samsung-ro, Yeongtong-gu, Suwon-si
Gyeonggi-do 443-803, Republic of Korea

DOI: 10.1002/admi.201500678

solid. In addition, PEDOT:PSS can be dissociated into PSS salt and PEDOT at higher pH levels (pH > 9); thus, PEDOT:PSS is easily aggregated when the pH of its solution is varied. The aggregated particles of PEDOT:PSS in the solution would form serious defects in the film morphology. Therefore, water-soluble conducting polymers with a high WF and fewer film defects are essentially required for the fabrication of highly efficient, flexible SP-PHJ PrSCs.

Among various conducting polymers, polyaniline (PANI) has been used as an efficient HTM in OLEDs[31–34] and improves hole injection to the emitting layer,[35,36] and exhibits high transmittance compared to that of PEDOT.[37] A water-soluble, self-doped conducting polyaniline graft copolymer, poly(4-styrenesulfonate)-*g*-polyaniline (PSS-*g*-PANI), can be a good material candidate as a HTM.[38] Unlike dispersible PEDOT:PSS, soluble PSS-*g*-PANI can steadily remain as an initial solution without aggregation during long-term storage and over a wide pH range because the grafted polymeric dopant, PSS, is covalently bonded to the conducting polymer chain PANI.[39] Moreover, the WF and conductivity of PSS-*g*-PANI can be tuned via the manipulation of the molecular ratio between the grafted PSS and the PANI during the synthesis process.[30]

In this study, we synthesized a self-doped conducting polymer, PSS-*g*-PANI, which is soluble in water and other polar solvents such as dimethyl formamide (DMF), and compared the bimolecular recombination in the device with PEDOT:PSS or PSS-*g*-PANI. In addition to the grafted PSS chains, we added an electron-withdrawing perfluorinated ionomer (PFI) into the PSS-*g*-PANI solution to increase the WF of PSS-*g*-PANI:PFI layer. We investigated the WF of the PSS-*g*-PANI and PSS-*g*- PANI:PFI hole-extraction layers (HELs) and their energy alignment with $MAPbI_3$; we then estimated the resulting energy barriers at the HEL/$MAPbI_3$ interface to explain the increased built-in potential (V_{bi}) and corresponding open-circuit voltage (V_{oc}) in the device with PSS-*g*-PANI and PSS-*g*- PANI:PFI. We also investigated the external quantum efficiency (EQE) and short-circuit current density (J_{sc}) of the device with PSS-*g*-PANI and observed that these parameters were correlated with high transmittance at the spectral response of $MAPbI_3$ PrSC with PSS-*g*-PANI compared to that with conventional PEDOT:PSS.

2. Results and Discussion

We followed the previously reported reaction procedure to synthesize PSS-*g*-PANI.[39] The product, PSS-*g*-PANI, was obtained with 1:6 PANI-to-PSS feeding ratio, as shown in **Figure 1**. We investigated the current density versus voltage (*J*–*V*) characteristics of the $MAPbI_3$ device fabricated using PSS-*g*-PANI or PEDOT:PSS under various light intensities ranging 100–1.5 mW cm^{-2} (**Figure 2**a,b). The PSS-*g*-PANI affects the shape of the *J*–*V* curve, which is strongly correlated with the recombination mechanism. At short circuit, the bimolecular recombination should be minimal for maximum carrier sweep out.[40] Figure 2c shows J_{sc} versus *I* plotted on a log–log scale and the fitted power law based on the following equation

$$J_{SC} \propto I^{\alpha} \ (\alpha \leq 1) \quad (1)$$

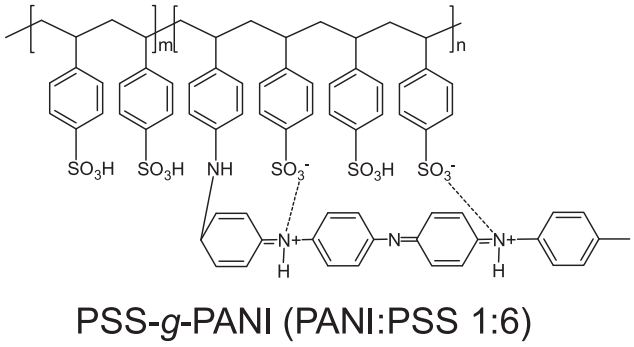

PSS-*g*-PANI (PANI:PSS 1:6)

Figure 1. Chemical structure of poly(4-styrenesulfonate)-*g*-polyaniline (PSS-*g*-PANI).

In principle, the observance of $\alpha = 1$ indicates that all the charge carriers have been removed prior to recombination. The α values of 0.926 and 0.962 were observed in the devices with PEDOT:PSS and PSS-*g*-PANI, respectively. Because deviation from $\alpha = 1$ is attributed to nongeminate recombination[41] and space charge effects,[42,43] the higher α of the device with PSS-*g*-PANI implies that the bimolecular recombination is close to minimal, which is correlated with the increase in the shunt resistance and high collection probability in the device.

The *J*–*V* characteristics of the perovskite photovoltaic cells with an indium–tin oxide (ITO)/HEL(PEDOT:PSS or PSS-*g*-PANI)/$MAPbI_3$/Phenyl-C61-butyric acid methyl ester (PCBM)/Al structure were obtained under the irradiation of air mass (AM) 1.5 global simulated sunlight at an intensity of 100 mW cm^{-2} (**Figure 3**). We also investigated the device parameters summarized in **Table 1** for PrSCs with PEDOT:PSS and PSS-*g*-PANI. The $MAPbI_3$ perovskite device with PSS-*g*-PANI exhibited a higher V_{oc} (1.04 V) and J_{sc} (14.1 mW cm^2) than that with pristine PEDOT:PSS (V_{oc} = 0.923 V; J_{sc} = 11.8 mA cm^{-2}). The device with PSS-*g*-PANI exhibited a PCE of 9.7%, whereas the device with pristine PEDOT:PSS exhibited a PCE of 7.8%. We speculated that these device results stemmed from the low bimolecular recombination in the device using PSS-*g*-PANI HTM compared with that in the device using PEDOT:PSS, as shown in Figure 2. However, the V_{oc} of the device with PSS-*g*-PANI was not the highest achieved among $MAPbI_3$ PrSCs; therefore, we used a perfluorinated polymeric acid dopant (i.e., PFI) to match the energy level of PSS-*g*-PANI to that of $MAPbI_3$ perovskite. The WF of a conducting polymer mixed with PFI is increased[44] according to previous density functional theory calculations;[28] therefore, we mixed PFI with PSS-*g*-PANI solution to achieve a high-WF HEL.[38] In addition, the PFI self-organizes at the surface of the PSS-*g*-PANI:PFI films by single spin-coating of the mixed solution due to the fluorinated moiety.[38,40] The *J*–*V* and device characteristics of the perovskite photovoltaic cells with an ITO/PSS-*g*-PANI:PFI/$MAPbI_3$/PCBM/Al structure are investigated in Figure 3 and Table 1. The V_{oc} (1.07 V), J_{sc} (14.9 mA cm^{-2}), and fill factor (FF) (77.5%) of the device were also increased compared with those of the device fabricated using PSS-*g*-PANI; therefore, PCE was increased to 12.4% in the device with PSS-*g*-PANI:PFI.

We compared the ultraviolet (UV) photoemission spectroscopy (UPS) results of PEDOT:PSS, PSS-*g*-PANI, and PSS-*g*-PANI:PFI (**Figure 4**) to investigate the energy level and

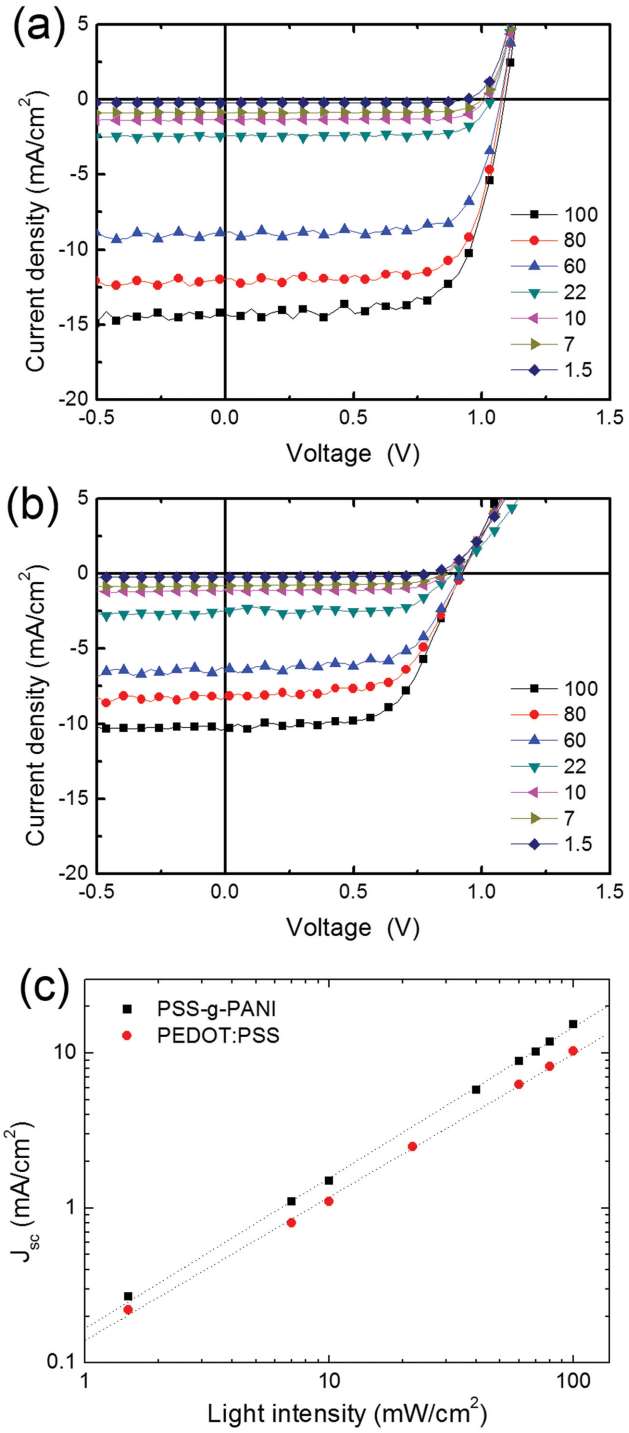

Figure 2. The *J–V* characteristics of the device with a) PSS-*g*-PANI and b) PEDOT:PSS under various light intensities ranging from 100 to 1.5 mW cm^{-2}. c) Measured J_{sc} of the device on the logarithmic scale and fitted power law (line) yield α.

electronic structure of conducting polymer (i.e., PEDOT or PANI) films with dopant polymers (i.e., PSS or PFI). We obtained the WF values of PEDOT:PSS (4.94 eV) and PSS-*g*-PANI (4.99 eV) from the secondary cutoff of the UPS spectra (left side of Figure 4). The WF values of PEDOT:PSS and PSS-*g*-PANI

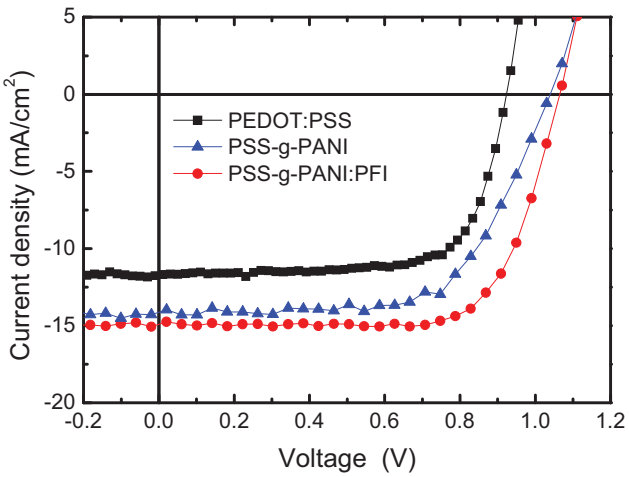

Figure 3. The *J–V* characteristics of the device with PEDOT:PSS, PSS-*g*-PANI, and PSS-*g*-PANI:PFI.

are similarly lower than the ionization energy (IE) of $MAPbI_3$ perovskite (5.43 eV); consequently, energy level offsets are formed at their interface with $MAPbI_3$ perovskite. However, despite the similar WFs of PEDOT:PSS and PSS-*g*-PANI, the V_{oc} of the device with PSS-*g*-PANI was higher than PEDOT:PSS (Figure 3). To investigate the higher V_{oc} of PSS-*g*-PANI, we analyzed the electronic structure of PEDOT:PSS and PSS-*g*-PANI films near the Fermi-energy level (right side of Figure 4). The density of filled (valence) states near the Fermi-energy level of PEDOT:PSS decreases with excess surface-enriched PSS molecules; thus, the density of filled states of PEDOT:PSS at the surface is downshifted to 0.25 eV below the Fermi-energy level.[45] In the case of self-doped PSS-*g*-PANI, the density of filled states near the Fermi-energy level is downshifted further to a deeper level than that of the conventional PEDOT:PSS (right side of Figure 4). In addition, we also compared the energy level and electronic structure of PSS-*g*-PANI:PFI. In previous research, the calculated IE of fluorinated ionomer has been reported to be higher than that of hydrocarbon ionomer because fluorinated moiety exhibits greater electron-withdrawing ability than hydrocarbon moiety and the oxidation of a fluorocarbon ionomer is more difficult than that of hydrocarbon ionomer.[28] Because the density of filled states close to the Fermi-energy level of PSS-*g*-PANI:PFI is more suppressed by the stronger electron-withdrawing PFI than the PSS (right side of Figure 4), the surface energy state is significantly downshifted below the Fermi-energy level and forms at a deeper level than that of PSS-*g*-PANI. As a result, PFI molecules can increase the surface

Table 1. The device characteristics of the device with PEDOT:PSS, PSS-*g*-PANI, and PSS-*g*-PANI:PFI.

	V_{oc} [V]	J_{sc} [mA cm–2]	FF [%]	PCE [%]	R_{sh} [Ω cm2]	R_s [Ω cm2]
PEDOT:PSS	0.923	11.8	73	7.8	1351	8.9
PSS-*g*-PANI	1.04	14.1	67.3	9.7	2969	13.1
PSS-*g*-PANI:PFI	1.07	14.9	77.6	12.4	37374	8.4

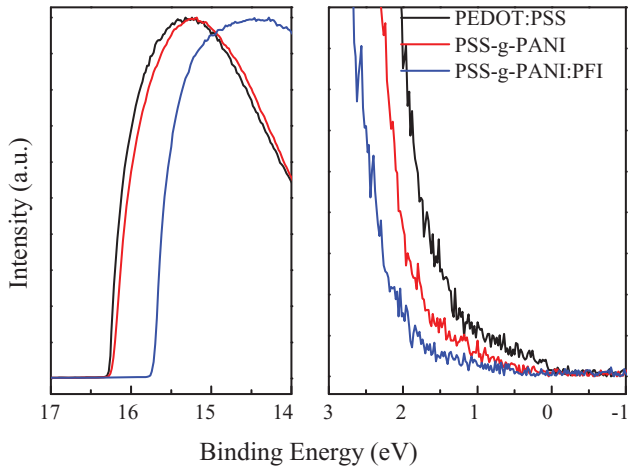

Figure 4. Ultraviolet photoelectron spectroscopy of PEDOT:PSS, PSS-*g*-PANI, and PSS-*g*-PANI:PFI.

WF and the surface energy state of PSS-*g* -PANI:PFI simultaneously.

The electronic structures of HELs are summarized in **Figure 5** as schematic diagrams of the Fermi-energy levels and the surface energy states of PEDOT:PSS, PSS-*g*-PANI, and PSS-*g*-PANI:PFI. The WF of PSS-*g*-PANI is similar to that of PEDOT:PSS; however, the surface energy state of PSS-*g*-PANI is formed at a deeper level than that of PEDOT:PSS. Moreover, PSS-*g*-PANI:PFI shows the higher WF and the deeper surface energy state compared to PEDOT:PSS and PSS-*g*-PANI. As a result, the energy offset between the surface energy state of PSS-*g*-PANI:PFI and the VBM of $MAPbI_3$ (–5.43 eV) is perfectly eliminated and forms an ohmic contact at the interface.[9–38] Therefore, we expect that the V_{bi} and corresponding V_{oc} in the device approach their maximum values because the potential loss of photogenerated charge is minimized at the interface between PSS-*g*-PANI:PFI and $MAPbI_3$.[44a]

To compare the V_{bi} of the PSS-*g*-PANI:PFI/$MAPbI_3$ PrSCs with that of the conventional PEDOT:PSS/$MAPbI_3$, we investigated the effect of the PSS-*g*-PANI:PFI by measuring the capacitance–voltage (*C*–*V*) characteristics in **Figure 6**a. The accumulated space charges inside the device can increase its

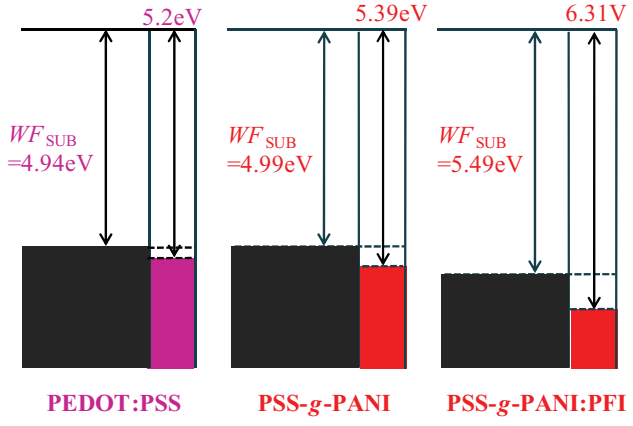

Figure 5. Schematic diagrams of energy level of PEDOT:PSS, PSS-*g*-PANI, and PSS-*g*-PANI:PFI.

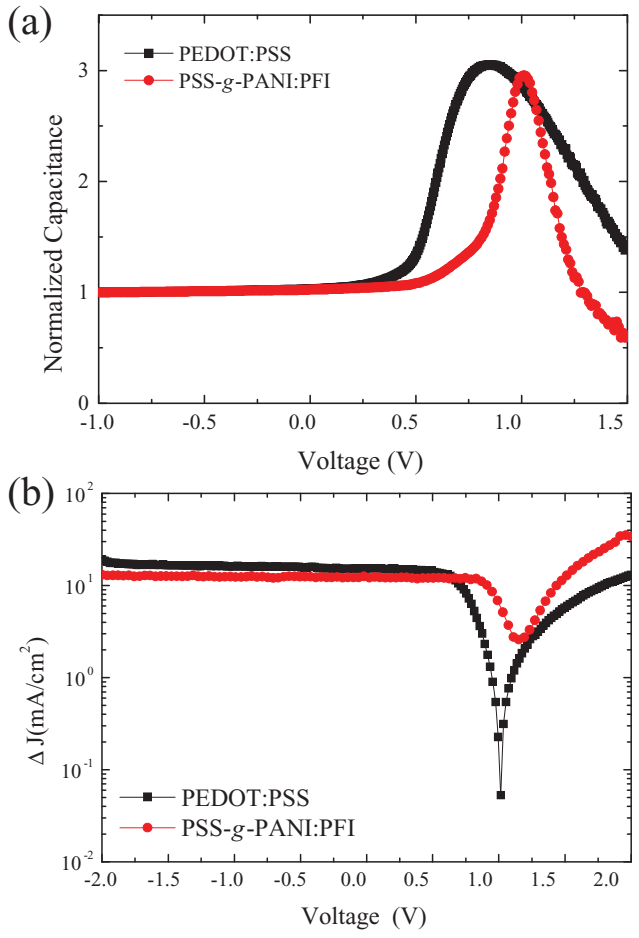

Figure 6. a) Capacitance–voltage and b) the difference of photocurrent between under illumination and in the dark (ΔJ) versus voltage of the devices with PEDOT:PSS and PSS-*g*-PANI:PFI.

capacitance. As the applied voltage increases, the capacitance tends to increase to a maximum and then decreases. The V_{bi} is correlated with the voltage V_{peak} at the peak capacitance as[9]

$$V_{bi} - V_{peak} \propto \frac{k_B T}{e} \tag{2}$$

where k_B is the Boltzmann constant, T is the absolute temperature, and e is the magnitude of the electron charge. Because V_{peak} is directly correlated with V_{bi}, a higher V_{peak} implies a higher V_{bi}, and thus, consequently a higher V_{oc}. The V_{peak} of PSS-*g*-PANI:PFI/$MAPbI_3$ PrSCs (1.01 V) was higher than that of their PEDOT:PSS/$MAPbI_3$ counterparts (0.85 V); this difference indicates that using PSS-*g*-PANI:PFI instead of conventional PEDOT:PSS increases the V_{oc} of the device.

We also measured the net photocurrent density (i.e., the difference, ΔJ, of photocurrent between under illumination and in the dark) in Figure 6b. The compensation voltage V_0 at which $\Delta J = 0$ is correlated with V_{bi}[9]

$$V_0 = V_{bi} - \frac{k_B T}{e} \ln(A) \tag{3}$$

where A is a material parameter. The higher V_0 of the PSS-*g*-PANI:PFI/$MAPbI_3$ device (V_0 = 1.15 V) compared with that of the PEDOT:PSS/$MAPbI_3$ device (1.01 V) is owing to the increased forward diffusion of photogenerated carriers in the PSS-*g*-PANI:PFI/$MAPbI_3$ device. This increased carrier diffusion in the PSS-*g*-PANI:PFI/$MAPbI_3$ device stems from the higher V_{bi} in the device than that in the PEDOT:PSS/$MAPbI_3$ device. Therefore, the compensation voltage analysis also reveals a high V_{bi} and consequently a higher V_{oc} in the PSS-*g*-PANI:PFI/$MAPbI_3$ device compared with conventional PEDOT:PSS/$MAPbI_3$ device (Figure 3). The PrSCs based on PSS-*g*-PANI showed the enhanced V_{oc} compared with PEDOT:PSS due to the deepened surface energy state of PSS-*g*-PANI (Figure 4); however, FF was reduced to 67.3% due to the partial dissolution of conducting polymers during PbI_2 deposition. PSS-*g*-PANI molecules are more soluble in polar organic solvents due to polar moieties in polymeric chain[39] compared to phase-segregated insoluble PEDOT molecules under the PSS-rich surface layer of PEDOT:PSS.[25,28] Therefore, series resistance (R_s) of the PrSCs based on PSS-*g*-PANI (13.1 Ω cm^2) was higher than that of device on PEDOT:PSS (8.9 Ω cm^2) due to the slight dissolution and morphological change of the PSS-*g*-PANI film by polar solvent (DMF) of PbI_2. However, FF of the PrSCs based on PSS-*g*-PANI:PFI was increased to 77.6% because the vertically phase-segregated and hydrophobic PFI-rich surface layer[29] of PSS-*g*-PANI:PFI could protect PSS-*g*-PANI from dissolution by DMF.

We compared the transmittances of PEDOT:PSS, PSS-*g*-PANI, and PSS-*g*-PANI:PFI to investigate EQE and the J_{sc} characteristics in the devices. The EQE spectra of the PSS-*g*-PANI:PFI/$MAPbI_3$ device exhibited 73% at the maximum, whereas that of the PEDOT:PSS/$MAPbI_3$ device showed 64% (**Figure 7**). The photocurrent integrated from the overlap of the EQE spectrum with the AM 1.5 G solar irradiation gives current density values of 14.78 and 12.26 mA cm^{-2} for the devices with PSS-*g*-PANI:PFI and PEDOT:PSS, respectively. The integrated photocurrent from EQE is consistent with the results of *J*–*V* characteristics in Figure 3 and Table 1. The high J_{sc} of the devices with PSS-*g*-PANI:PFI is affected not only by well-aligned energy levels in the PSS-*g*-PANI:PFI/$MAPbI_3$ device but also by the higher transmittance of PSS-*g*-PANI than PEDOT:PSS (**Figure 8**). The $MAPbI_3$ solar cell exhibits the spectral response of the device from the visible to near-infrared (i.e., 300–800 nm) region in Figure 7; the transmittances of the PSS-*g*-PANI and PSS-*g*-PANI:PFI films are substantially greater in this near-infrared region compared with that of the conventional PEDOT:PSS. Therefore, the J_{sc} characteristics in the device with PSS-*g*-PANI and PSS-*g*-PANI:PFI were increased compared with conventional PEDOT:PSS.

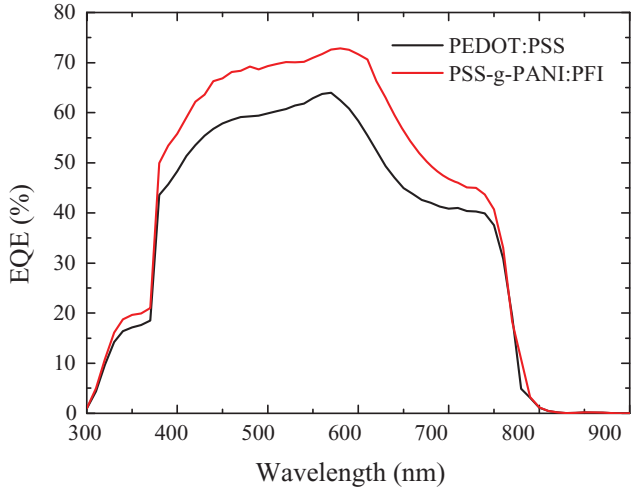

Figure 7. EQE spectra of the device with PEDOT:PSS and PSS-*g*-PANI:PFI.

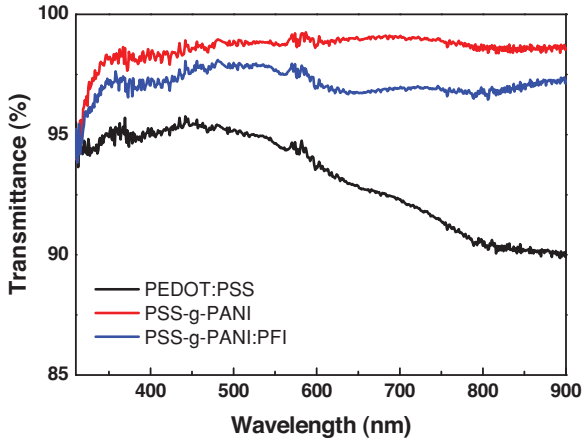

Figure 8. Transmittance of the PEDOT:PSS, PSS-*g*-PANI, and PSS-*g*-PANI:PFI films.

3. Conclusion

A water-soluble self-doped PSS grafted polyaniline copolymer (PSS-*g*-PANI) was used to achieve high PCE in SP-PHJ PrSCs. The PSS-*g*-PANI achieves a good energy level alignment with the VBM of $MAPbI_3$ and high transmittance at the spectral response of $MAPbI_3$; it consequently improves device characteristics, such as the V_{oc} and J_{sc}, of SP-PHJ $MAPbI_3$ PrSCs. Moreover, when the strong electron-withdrawing PFI was added to PSS-*g*-PANI, the PSS-*g*-PANI:PFI film exhibited a higher WF and the more downshifted surface energy state below the Fermi-energy level due to greater electron-withdrawing ability of PFI than hydrocarbon. As a result of the sufficiently deep surface energy state of PSS-*g*-PANI:PFI for VBM of $MAPbI_3$ perovskite, the energy offset at the interface with the $MAPbI_3$ was eliminated and thereby resulting potential loss in the device at the interface was reduced. Moreover, the transmittances of the PSS-*g*-PANI and PSS-*g*-PANI:PFI films are substantially greater in the absorption spectra of the device compared to that of the conventional PEDOT:PSS. Therefore, the PCE was increased from 7.8% in the $MAPbI_3$ perovskite solar cell with PEDOT:PSS to 12.4% in that with PSS-*g*-PANI:PFI. We believe that our work provides a crucial insight into developing hole transporting interlayer in SP-PHJ PrSCs and furthermore important way to overcome the critical potential loss problem which is universally found in SP-PHJ PrSCs.

4. Experimental Section

Synthesis of PSS-g-PANI: First, di-tert-butyloxy dicarbonate, $(BOC)_2O$ (12.5 mmol) and triethylamine (12.5 mmol) were dissolved to a solution of p-aminostyrene (10.0 mmol) in dioxane (50 mL) and then the solution was mixed at 100 °C. Petroleum ether (150 mL) and deionized (DI) water (150 mL) were mixed in sequence after 15 h. The solid phase was separated, washed, and concentrated. BOC-aminostyrene (a white solid) was recrystallized in a yield of 50%. Second, P(SSNa-co-BOC-PMS) was copolymerized with sodium styrenesulfonate (SSNa) and BOC-aminostyrene by a radical initiator of 2,20-azo-*bis*(isobutyronitrile) (AIBN). SSNa (24.2 mmol) and BOC-aminostyrene (0.484 mmol) were dissolved in dimethyl sulfoxide (DMSO) and then the temperature was increased to 80 °C. AIBN was added dropwise over 5 h under N_2 atmosphere. P(SSNa-co-BOC-PMS) was repeatedly precipitated, filtered, and washed with acetone, and dried in a vacuum at 60 °C for 48 h. Finally, 0.6 g of P(SSNa-co-BOC-PMS) was added to 30 mL of HCl aqueous solution (1 M) and 0.1 g (1.07 mmol) of aniline was added to the mixture in sequence. The mixture was stirred and then chilled at 0 °C, then 20 mL of ammonium persulfate (244 mg, 1.07 mmol) in 1 N HCl aqueous solution was added dropwise. After stirring for a few hours, the solution was filtered and purified by dialysis membrane. The product was precipitated by acetone and dried in a vacuum at 60 °C. PSS-*g*-PANI with the feeding ratio of PANI to PSS (1:6) was obtained.[30]

Device Fabrication: A solution of PSS-*g*-PANI was mixed with 5 wt% tetrafluoroethylene-perfluoro-3,6-dioxa-4-methyl-7-octene-sulfonic acid copolymer (PFI) (Sigma Aldich Co.) for PSS-*g*-PANI:PFI. PEDOT:PSS (Clevios PH), PSS-*g*-PANI, and PSS-*g*-PANI:PFI were spin-coated as a hole-extraction layer (30 nm thick) on top of ITO/glass. These layers were baked on a hotplate in air at 150 °C for 10 min. The substrates were moved to an N_2 glove box, then a PbI_2 layer was spin-cast from 17.2 wt% PbI_2 solution in anhydrous *N*,*N*-dimethylformamide (Aldrich) with a spin-coating speed of 8000 rpm for 30 s, followed by thermal annealing 70 °C for 10 min. CH_3NH_3I was deposited from 20 mg mL^1 CH_3NH_3I solution in anhydrous Isopropyl alcohol (IPA) with spin-coating speed of 3000 rpm for 30 s; the film immediately darkened after the CH_3NH_3I solution was added. The coated films were then placed on a hot plate set at 100 °C for 5 min. The PCBM layer was spin-coated from 0.7 wt% PCBM (nano-C Inc.) solution in chloroform, then cathodes were thermally evaporated on the photoactive layer surface in a vacuum (2×10^{-7} Torr). A 20 nm Al cathode layer was deposited at 1Å s^{-1} and an 80 nm Al cathode layer was deposited at 3 Å s^{-1} sequentially. The photoactive area (0.06 cm^2) was determined using metallic shadow masks. In the N_2 glove box, an UV-curable epoxy resin was used to encapsulate the devices with a glass lid.

Characterization: The current density–voltage characteristics (*J*–*V* curves) were obtained using a Keithley 2400 source measurement unit under irradiation at AM-1.5 100 mW cm^{-2} generated using a Newport 69907 solar simulator.

The WF of surface was measured using UPS. All measurements were conducted at room temperature.

Acknowledgements

This work was supported by the Agency for Defense Development (UD140044GD), Republic of Korea.

Received: October 26, 2015
Revised: December 26, 2015
Published online: February 10, 2016

[1] A. Kojima, K. Teshima, Y. Shirai, T. Miyasaka, *J. Am. Chem. Soc.* **2009**, *131*, 6050.
[2] H. S. Kim, J. W. Lee, N. Yantara, P. P. Boix, S. A. Kulkarni, S. Mhaisalkar, M. Grätzel, N. G. Park, *Nano Lett.* **2013**, *13*, 2412.
[3] J. H. Heo, S. H. Im, J. H. Noh, T. N. Mandal, C. S. Lim, J. A. Chang, Y. H. Lee, H. Kim, A. Sarkar, M. K. Nazeeruddin, M. Grätzel, S. I. Seok, *Nat. Photonics* **2013**, *7*, 486.
[4] J. Burschka, N. Pellet, S.-J. Moon, R. Humphry-Baker, P. Gao, M. K. Nazeeruddin, M. Grätzel, *Nature* **2013**, *499*, 316.
[5] M. M. Lee, J. Teuscher, T. Miyasaka, T. N. Murakami, H. J. Snaith, *Science* **2012**, *338*, 643.
[6] M. Liu, M. B. Johnston, H. J. Snaith, *Nature* **2013**, *501*, 395.
[7] P.-W. Liang, C.-Y. Liao, C.-C. Chueh, F. Zuo, S. T. Williams, X.-K. Xin, J. Lin, A. K.-Y. Jen, *Adv. Mater.* **2014**, *26*, 3748.
[8] G. E. Eperon, V. M. Burlakov, P. Docampo, A. Goriely, H. J. Snaith, *Adv. Funct. Mater.* **2014**, *24*, 151.
[9] a)K.-G. Lim, H.-B. Kim, J. Jeong, H. Kim, J. Y. Kim, T.-W. Lee, *Adv. Mater.* **2014**, *26*, 6461; b) K.-G. Lim, S. Ahn, Y.-H. Kim, Y. B. Qi, T.-W. Lee,*Energy Environ. Sci.* **2016**, 10.1039/c5ee03560k.
[10] a) W. S. Yang, J. H. Noh, N. J. Jeon, Y. C. Kim, S. Ryu, J. Seo, S. I. Seok, *Science* **2015**, *348*, 1234; b) H. Kim, K.-G. Lim, T.-W. Lee,*Energy Environ. Sci.* **2016**, *9*, 12.
[11] C. R. Kagan, D. B. Mitzi, C. D. Dimitrakopoulos, *Science* **1999**, *286*, 945.
[12] K. Tanaka, T. Takahashi, T. Ban, T. Kondo, K. Uchida, N. Miura, *Solid State Commun.* **2003**, *127*, 619.
[13] Y.-H. Kim, H. Cho, J. H. Heo, T.-S. Kim, N. Myoung, C.-L. Lee, S. H. Im, T.-W. Lee, *Adv. Mater.* **2015**, *7*, 1248.
[14] J. H. Im, C. R. Lee, J. W. Lee, S. W. Park, N. G. Park, *Nanoscale* **2011**, *3*, 4088.
[15] J.-Y. Jeng, K.-C. Chen, T.-Y. Chiang, P.-Y. Lin, T.-D. Tsai, Y.-C. Chang, T.-F. Guo, P. Chen, T.-C. Wen, Y.-J. Hsu, *Adv. Mater.* **2014**, *26*, 4107.
[16] J. Y. Jeng, Y. F. Chiang, M. H. Lee, S. R. Peng, T. F. Guo, P. Chen, T. C. Wen, *Adv. Mater.* **2013**, *25*, 3727.
[17] Z. Wu, S. Bai, J. Xiang, Z. Yuan, Y. Yang, W. Cui, X. Gao, Z. Liu, Y. Jin, B. Sun, *Nanoscale* **2014**, *6*, 10505.
[18] J.-S. Yeo, R. Kang, S. Lee, Y.-J. Jeon, N. Myoung, C.-L. Lee, D.-Y. Kim, J.-M. Yun, Y.-H. Seo, S.-S. Kim, S.-I. Na, *Nano Energy* **2015**, *12*, 96.
[19] D. Zhao, M. Sexton, H.-Y. Park, G. Baure, J. C. Nino, F. So, *Adv. Energy Mater.* **2015**, *5*, 1401855.
[20] T. Krishnamoorthy, F. Kunwu, P. P. Boix, H. Li, T. M. Koh, W. L. Leong, S. Powar, A. Grimsdale, M. Grätzel, N. Mathews, S. G. Mhaisalkar, *J. Mater. Chem. A: Mater. Energy Sustain.* **2014**, *2*, 6305.
[21] Q. Lin, A. Armin, R. C. R. Nagiri, P. L. Burn, P. Meredith, *Nat. Photonics* **2015**, *9*, 106.
[22] K.-G. Lim, M.-R. Choi, J. H. Kim, D. H. Kim, G. H. Jung, Y. Park, J.-L. Lee, T.-W. Lee, *ChemSusChem* **2014**, *7*, 1125.
[23] K.-G. Lim, J.-M. Park, H. Mangold, F. Laquai, T.-L. Choi, T.-W. Lee, *ChemSusChem* **2015**, *8*, 337.
[24] a) K.-G. Lim, M.-R. Choi, H. Kim, J. H. Park, T.-W. Lee, *J. Mater. Chem.* **2012**, *22*, 25148; b) T.-W. Lee, K.-G. Lim, D.-H. Kim, *Electron. Mater. Lett.* **2010**, *6*, 41.
[25] D.-H. Kim, K.-G Lim, J. H. Park, T.-W. Lee, *ChemSusChem* **2012**, *5*, 2053.
[26] S. Kwon, K.-G. Lim, M. Shim, H. C. Moon, J. Park, G. Jeon, J. Shin, K. Cho, T.-W. Lee, J. K. Kim, *J. Mater. Chem. A: Mater. Energy Sustain.* **2013**, *1*, 11802.
[27] G. H. Jung, K.-G. Lim, T.-W. Lee, J.-L. Lee, *Sol. Energy Mater. Sol. Cells* **2011**, *95*, 1146.
[28] T.-W. Lee, Y. Chung, *Adv. Funct. Mater.* **2008**, *18*, 2246.
[29] T.-W. Lee, Y. Chung, O. Kwon, J. J. Park, *Adv. Funct. Mater.* **2007**, *17*, 390.
[30] D. H. Huh, M. Chae, W. J. Bae, W. H. Jo, T.-W. Lee, *Polymer* **2007**, *48*, 7236.
[31] H. L. Wang, A. G. MacDiarmid, Y. J. Wang, D. D. Gebler, A. J. Epstein, *Synth. Met.* **1996**, *78*, 33.

[32] S. A. Carter, M. Angelopous, S. Karg, P. J. Brock, J. C. Scott, *Appl. Phys. Lett.* **1997**, *70*, 2067.
[33] S. Karg, J. C. Scott, J. R. Salem, M. Angelopoulos, *Synth. Met.* **1996**, *80*, 111.
[34] M.-R. Choi, S.-H. Woo, T.-H. Han, K.-G. Lim, S.-Y. Min, W. M. Yun, O. K. Kwon, C. E. Park, K.-D. Kim, H.-K. Shin, M.-S. Kim, T. Noh, J. H. Park, K.-H. Shin, J. Jang, T.-W. Lee, *ChemSusChem* **2011**, *4*, 363.
[35] Y. Yang, A. J. Heeger, *Appl. Phys. Lett.* **1994**, *64*, 1245.
[36] G. Gustafsson, Y. Cao, G. M. Treacy, F. Klavetter, N. Colaneri, A. J. Heeger, *Nature* **1992**, *357*, 477.
[37] J. Jang, J. Ha, K. Kim, *Thin Solid Films* **2008**, *516*, 3152.
[38] M.-R. Choi, T.-H. Han, K.-G. Lim, S.-H. Woo, D. H. Huh, T.-W. Lee, *Angew. Chem. Int. Ed. Engl.* **2011**, *50*, 6274.
[39] W. J. Bae, K. H. Kim, Y. H. Park, W. H. Jo, *Chem. Commun.* **2003**, *22*, 2768.
[40] R. A. Street, M. Schoendorf, A. Roy, J. H. Lee, *Phys. Rev.B: Condens. Matter* **2010**, *81*, 205307.
[41] L. Ye, S. Zhang, W. Ma, B. Fan, X. Guo, Y. Huang, H. Ade, J. Hou, *Adv. Mater.* **2012**, *24*, 6335.
[42] Z. Li, F. Gao, N. C. Greenham, C. R. McNeill, *Adv. Funct. Mater.* **2011**, *21*, 1419.
[43] M. Lenes, M. Morana, C. J. Brabec, P. W. M. Blom, *Adv. Funct. Mater.* **2009**, *19*, 1106.
[44] a) Y. Zhu, T. Song, F. Zhang, S.-T. Lee, B. Sun, *Appl. Phys. Lett.* **2013**, *102*, 113504; b) H. Cho, S.-H. Jeong, M.-H. Park, Y.-H. Kim, C. Wolf, C.-L. Lee , J. H. Heo, A. Sadhanala, N. Myoung, S. Yoo, S. H. Im, R. H. Friend, T.-W. Lee, *Science* **2015**, *350*, 1222; c) Y.-H. Kim, H. Cho, J. H. Heo, T.-S. Kim, N. Myoung, C.-L. Lee, S. H. Im, T.-W. Lee, *Adv. Mater* **2015**, *27*, 1248.
[45] J. Hwang, F. Amy, A. Kahn, *Org. Electron.* **2006**, *7*, 387.

